Assessment of future wind speed and wind power changes over South Greenland using the MAR regional climate model

Clara Lambin[1], Xavier Fettweis[1], Christoph Kittel[1,2], Michaël Fonder[3], and Damien Ernst[3,4]

[1] *Department of Geography, University of Liège, Liège, Belgium*
[2] *Université Grenoble Alpes/CNRS/IRD/G-INP, IGE, Grenoble, France*
[3] *Department of Electrical Engineering and Computer Science, University of Liège, Liège, Belgium*
[4] *LTCI, Telecom Paris, Institut Polytechnique de Paris, Paris, France*

Abstract

Wind is an infinitely renewable energy source that is not evenly distributed in space and time. The interconnection of energy-demanding and energy-resourceful (yet remote) regions would help preventing energy scarcity in a world where fossil fuels are no longer used. Previous studies have shown that South Greenland and West Europe have complementary wind regimes. In particular, the southern tip of Greenland, Cape Farewell, has gained growing interest for wind farm development as it is one of the windiest places on Earth. In order to gain new insights about future wind speed variations over South Greenland, the Modèle Atmosphérique Régional (MAR), validated against *in situ* observations over the tundra where wind turbines are most likely to be installed, is used to built climate projections under the emission scenario SSP5-8.5 by downscaling an ensemble of CMIP6 Earth System Models (ESMs). It appeared that between 1981 and 2100, the wind speed is projected to decrease by ∼-0.8 m/s at 100 m a.g.l. over the tundra surrounding Cape Farewell. This decrease is particularly marked in winter while in summer, a wind speed accelaration is projected along the ice sheet margins. An analysis of two-dimensional wind speed changes at different vertical levels indicates that the winter decrease is likely due to a large-scale circulation change while in summer, the katabatic winds flowing down the ice sheet are expected to increase due to an enhanced temperature contrast between the ice sheet and the surroundings. As for the mean annual maximum wind power a turbine can yield, a decrease of ∼-178.1 W is projected at 100 m a.g.l. Again, the decrease is especially pronounced in winter. Considering the very high winter wind speeds occurring in South Greenland which can cut off wind turbines if too intense, the projected wind speed decrease might be beneficial for the establishment of wind farms near Cape Farewell.

1 Introduction

Global warming is one of the most important challenges of the 21st century and its mitigation requires, among others, replacing fossil fuels with renewable energy sources. Wind offers an advantage as it is infinitely renewable and non-polluting. Nonetheless, wind speeds required for efficient power harvesting are not equally distributed across the globe and over time (Radu et al., 2019). Moreover, the distribution of the energy demand is not spatially uniform. As a result, some countries, especially the densely populated ones, do not have within their limits the sufficient renewable energy potential to satisfy their local demand (Berger et al., 2021). Therefore, different concepts have emerged to address this issue. Firstly, the concept of a "global grid" proposes linking regions with complementary wind regimes in order to build a reliable worldwide power system (Chatzivasileiadis et al., 2013). The main idea is to connect energy-demanding and energy-producing regions with long-distance power transmission lines that have been proven to be both technologically and economically feasible. By doing so, the intermittency issue of wind resources at a given place would be addressed by providing electricity from a high yielding area in times of need. Because of the low local demand, exploiting the renewable energy potential of a remote resourceful area allows a large part of the generated electricity to be directly exported to high-demanding regions. Secondly, the concept of "remote renewable hubs" suggests that this electricity could be used to produce on-site carbon-neutral synthetic fuels that are then to be exported as well to high-demanding regions, as discussed in Berger et al. (2021).

In terms of wind power harvesting, the southern tip of Greenland, Cape Farewell (Fig. 1), has been identified as a highly resourceful yet remote region (da Silva Soares, 2016; Jakobsen, 2016; Radu et al., 2019). It is one of the windiest places on Earth due to the specific action of the Greenland Ice Sheet (GrIS) on the synoptic flow due to the presence of the Icelandic Low and the presence of cold katabatic winds flowing down the ice sheet (Moore et al., 2015). Moreover, it appears that the temporal variability of the wind in this region is complementary with the European wind regime (Radu et al., 2019). This means that in times of low wind power productivity, especially during summer, Europe could be supplied by Greenlandic wind farms to compensate for any energy production deficit with the implementation of this so-called global grid (Radu et al., 2019).

In order to exploit the Greenlandic wind resources for electricity production, not only is a good knowledge of the current wind speed field necessary, but there is also a need to have an idea how it will change in future. Because the Arctic is a region undergoing the strongest warming due to the Arctic Amplification (Serreze and Francis, 2006), a long-term wind speed variability analysis would enable one to assess if wind speed is likely to be affected by climate change and therefore if there are any suitable prospects for wind farm development. To perform such an evaluation, using high-resolution climate models such as regional climate models (RCM) is relevant as they provide a continuous representation of the wind speed field in time and space, which is particularly useful in Greenland, an observation-scarce region. Moreover, RCMs can project wind changes at high spatial resolution under different emission scenarios by downscaling low-resolution Earth System Models (ESMs). Although the wind speed field over Cape Farewell has already been evaluated by a few studies using different RCMs (e.g. Bromwich et al. 2001; Ettema et al. 2010b; Gorter et al. 2014; Jakobsen 2016; Klein et al. 2001), the long-term wind speed variability has not been comprehensively investigated at high spatial resolution. Gorter et al. (2014) used the Regional Atmospheric Climate Model (RACMO2) at a spatial resolution of 11 km to examine the change in the Weibull shape and scale parameters (which characterise the Weibull function of an asymmetrical distribution) of the wind speed distribution by the end of the 21st century, but only under the medium-range scenario of radiative forcing RCP4.5 (Radiative Concentration Pathway) from the Coupled Model Intercomparison Project phase 5 (CMIP5) (O'Neill et al., 2016).

In this study, the RCM Modèle Atmosphérique Régional (MAR), version 3.12, has been chosen to evaluate the long-term wind speed variability over South Greenland under a high-end scenario of radiative forcing (SSP (Shared Socioeconomic Pathway) 5-8.5 from CMIP6). MAR has already been used multiple times over Greenland and has been proven to be well suited for the modelling of polar climates (e.g., Fettweis et al. 2013, 2017, 2020). Although MAR wind speed outputs have been evaluated on a daily scale above the GrIS by Delhasse et al. (2020), they have not been evaluated over the ice-free area (tundra) of Greenland, which is the relevant area to investigate as the ice sheet is not appropriate for the installation of wind turbines due to ice dynamics.

The main objective of this paper is thus to investigate future wind speed and wind power changes by the year 2100 over Cape Farewell by analysing trends over the study area from projections built with MAR forced with an ensemble of CMIP6 ESMs. Prior to this analysis, an evaluation of hourly MAR wind speed outputs over the Greenlandic tundra will be carried out by comparing the model outputs with observation data, including a new set of data acquired during the Belgian KATABATA expedition (Link to https://www.katabata-project.uliege.be/). Such an evaluation will provide good insights into whether or not the MAR-modelled wind speeds are reliable before performing the long-term wind speed analysis.

2 Wind regime in South Greenland

The wind regime in South Greenland is driven by the katabatic winds originating from the ice sheet which can interact with the synoptic flow induced by the Icelandic Low. Katabatic winds occur on sloping terrains and result from a negative radiation balance at the surface which causes a downward sensible heat flux from the subjacent air layer to compensate for this radiation deficit (van den Broeke et al., 1994). The latter is the result of the low heat absorption of the surface in short-wave radiation due to its high reflectivity combined with a lack of solar radiation and a relatively higher outgoing emission in long-wave radiation (Ettema et al., 2010b; van As et al., 2014). The downward sensible heat flux leads to the cooling of the near-surface air and generates an inversion layer (van den Broeke et al., 1994). The lowering temperature of the air increases its density and the layer becomes negatively buoyant, creating a horizontal pressure gradient along the slope that drives the cooled near-surface air downslope combined with the action of gravity (van den Broeke et al., 1994).

Over Greenland, the ice sheet cools the relatively warmer overlying air layer by radiative transfer and katabatic winds develop over a large part of it (Gorter et al., 2014). Katabatic winds are characterised through their almost constant directional flow going down the ice sheet (considering the deviation by the Coriolis force). Their intensity, as well as the thickness of the katabatic layer, depends on the steepness and length of the slope, the temperature gradient of the inversion layer and the surface roughness. Over the GrIS, the weakest katabatic winds are found at the top of the ice sheet where the slopes are gentle while the strongest are found near its margins, especially along the south-eastern coast, where the slopes are the steepest (Gorter et al., 2014; Jakobsen, 2016).

Concerning the synoptic flow over Cape Farewell, it is mainly influenced by the presence of the Icelandic Low, located offshore between Greenland and Iceland. The Icelandic Low is a climatological low-pressure system, which is the net effect of all the meteorological lows passing over the Irminger Sea (Fig. 1). The position of the Icelandic Low is close to the south-eastern coast of Greenland during winter, while it shifts closer to the southern coast of Iceland during the summer. Its intensity is stronger in winter than in summer (Ettema et al., 2010a). Because Greenland has a very high topography with its thick ice sheet that reaches 3 250 m above sea level (a.s.l.) (Jakobsen, 2016), the geostrophic flow associated with the low-pressure system is blocked and distorted by the orography. This leads to the creation of mesoscale low-level high wind speed events that are barrier winds and tip jets. Barrier winds occur along the coast of Greenland while tip jets occur at the tip of Cape Farewell. The wind speed maxima of these phenomena are located above the ocean but their strong wind speeds can influence the on-shore winds (Moore and Renfrew, 2005). Over land, the katabatic winds can also add to the synoptic flow when flowing downwards in the same direction, leading to high and constant wind speeds, as it is the case over the ice-free area of Cape Farewell (Klein and Heinemann, 2002; Radu

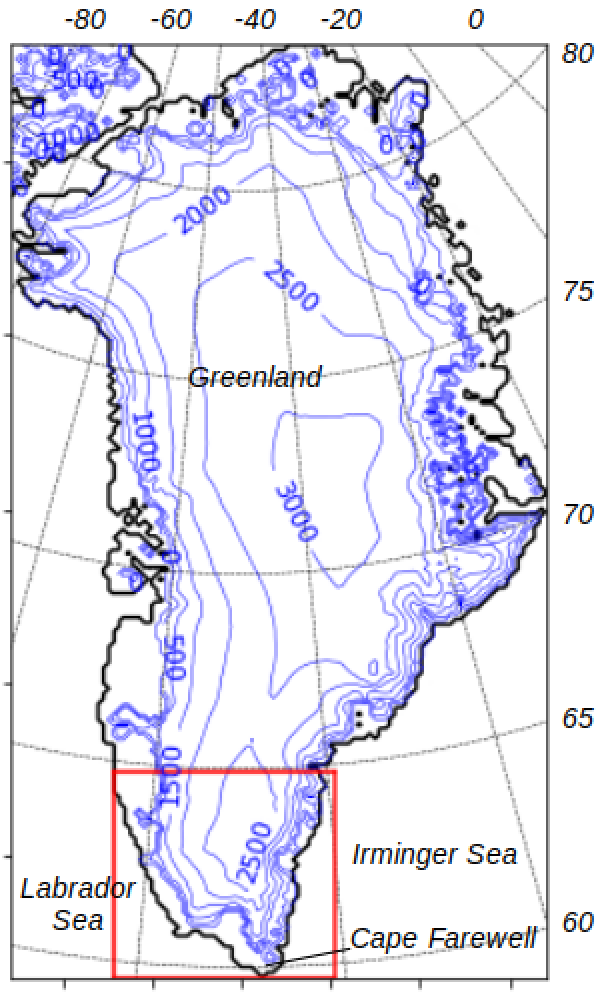

Figure 1: Greenland and surroundings modelled by MAR. The study area is represented by the red frame. The blue lines represent the ice sheet and its topography in meters.

et al., 2019).

3 Material and method

3.1 Study Area

The area of interest in this study is the southern tip of Greenland, Cape Farewell (Fig. 1). As explained previously, it is one of the windiest places on Earth as a consequence of a combination of katabatic winds from the GrIS with on-shore geostrophic winds and off-shore high-wind speed events such as tip jets and barrier winds. The selected area is located between 59.5°N and 64.5°N and between 40.0°W and 52.0°W.

3.2 Observation data

The observation data used for the evaluation of MAR are *in situ* measurements obtained from multiple weather stations located in the study area. These stations are displayed in Fig. 2 and are from three different databases: the Danish Meteorological Institute (DMI), the Program for Monitoring of the Greenland Ice Sheet (PROMICE) and the KATABATA project carried out by the University of Liège (Belgium). Details about the station locations are given in Table 1.

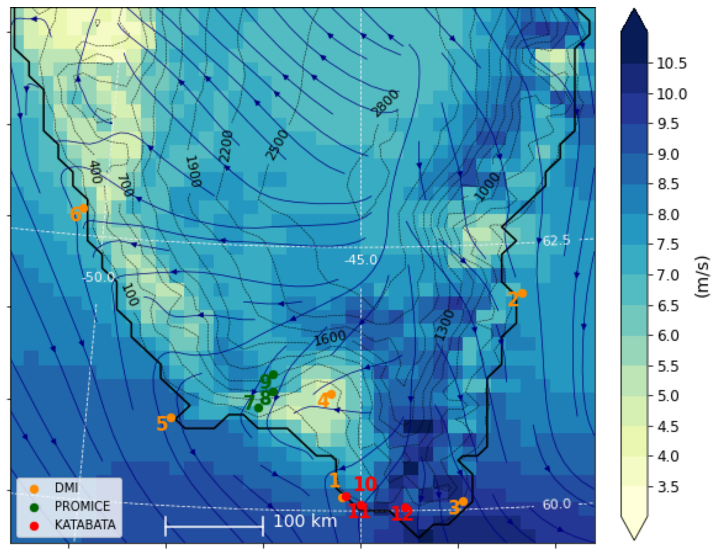

Figure 2: Mean wind speed (shaded colours), wind direction (streamlines) and station locations (coloured dots, see Table 1). The mean wind speed and direction were calculated on hourly data modelled by MAR from 2016 to 2018 forced with ERA-5.

The KATABATA project was developed and conducted by two research units, SPHERES and MONTEFIORE, from the University of Liège (ULiège) and aims at increasing the availability of *in situ* observations of katabatic winds at the southern tip of Greenland (https://www.katabata-project.uliege.be/). Therefore, three Finnish-made Vaisala automatic weather stations were installed in the ice-free area near Cape Farewell in September 2020. These stations have been established so as to be directly located in front of the prevailing winds, where previous MAR test simulations have identified wind speed maxima (Radu et al., 2019). The stations measure temperature, humidity and horizontal wind speed with readings transmitted every 20 minutes by satellite connection. The wind speed is measured at 10 m above ground level (a.g.l) and the temperature at 2 m a.g.l. The datasets from these stations range from September 2020 to the end of January 2021 for KAT 6640, the end of August 2021 for KAT 0460 and the end of February 2021 for KAT 0680. The time period differs from stations because some experienced a wind sensor failure during the winter of 2020/2021, but these problems have been resolved thanks to a maintenance visit in July 2021. The KATABATA project has been implemented in the context of the "global grid" and the potential connections that could be made between West Europe and South Greenland in terms of renewable energy supply. Although the KATABATA stations have been installed specifically to assess the katabatic wind potential of Cape Farewell and to enable the evaluation of model performances to simulate these winds, their time series are relatively short and representative of a narrow area to evaluate

Number	Station ID	Station name	Database	Longitude	Latitude	Elevation (m)
1	ANG	Angissoq	DMI	-45.1461	59.9911	4.38
2	IKM	Ikeramiuarsuk	DMI	-42.0678	61.9364	39.59
3	IKS	Ikerasassuaq	DMI	-43.1653	60.0553	88
4	NAR	Narsarsuaq	DMI	-45.4400	61.1575	3.9
5	NUN	Nunarssuit	DMI	-48.4544	60.7636	32.6
6	UKI	Ukiiviit	DMI	-50.4058	62.5789	22.23
7	QAS_L	QAS_L	PROMICE	-46.8493	61.0308	280
8	QAS_M	QAS_M	PROMICE	-46.833	61.0998	630
9	QAS_U	QAS_U	PROMICE	-46.8195	61.1753	900
10	KAT 6640	AWS 6640	KATABATA-ULiège	-45.1799	59.9842	36
11	KAT 0460	AWS 0460	KATABATA-ULiège	-45.0677	60.1567	76
12	KAT 0680	AWS 0680	KATABATA-ULiège	-44.0623	60.1833	11

Table 1: Detailed table of the station locations from Fig. 2

our MAR climate model in depth. This is why, in addition to time series from the KATABATA project, PROMICE and DMI data has been used in the evaluation of MAR hourly wind speed outputs.

The PROMICE stations are located directly on the GrIS and measure a series of variables including horizontal wind speed, sensor height and GPS location. The climatic variables are measured every 10 minutes and thereafter transmitted as hourly averages. The GPS data is recorded every 6 hours. Because the stations are located on the ice sheet where the snowfall accumulation is high, the height above the surface at which the wind speed is measured is variable, as the base of the station is gradually buried under snow during winter. Theoretically, the height measured by the sensor would be 3.1 m if the stations were not to sink into the snow (Fausto et al., 2021). Measured heights above ground, recorded every 6 hours, are provided in the PROMICE datasets. The PROMICE data used in this study are the third version of the hourly datasets of stations QAS_L, QAS_M and QAS_U for the years 2016, 2017 and 2018, except for QAS_M which has only been active since the 11th of August 2016 and which has a very incomplete dataset for 2017. Therefore, only the 2018 dataset was used for this station. This 2016-2018 time period was chosen because, together with the DMI stations, it has the most complete datasets for the selected stations.

The DMI stations (ANG, IKM, IKS, NAR, NUN and UKI, see Table 1) are located on the ice-free area surrounding the GrIS. In Fig. 2, some stations seem to be located directly in the ocean. This is due to their location on small islands along the coast that are not resolved by MAR at a 15 km resolution. These stations automatically record variables including wind speed, measured at 10 m a.g.l. every ten minutes (Cappelen et al., 2001). The datasets in the chosen time period were available for 2016, 2017 and 2018 for ANG, IKM, NUN and UKI, for 2016 and 2017 for IKS and were only available for 2018 for station NAR. For these stations, the wind gust data (mean highest 3-second wind speed over the past hour, measured at 10 m a.g.l.) was also available.

3.3 The MAR model

MAR is a 3D atmosphere-snowpack regional climate model coupled with the 1D SISVAT (Soil Ice Snow Vegetation Atmosphere Transfer) scheme which enables the modelling of surface processes (Gallée et al., 2013; Fettweis et al., 2017). A full description of the atmospheric part of MAR can be found in Gallée and Schayes (1994). The SISVAT scheme is described in De Ridder and Gallée (1998). A summary of the different modules and schemes used in MAR can be found in Fettweis et al. (2017). MAR has been used in multiple studies conducted over Greenland, especially for surface mass balance and surface melt investigation (e.g., Fettweis et al. 2013, 2017, 2020; Franco et al. 2012, 2013; Hanna et al. 2021; Payne et al. 2021). Its wind speed outputs have been studied over Greenland (Delhasse et al., 2020; Radu et al., 2019) and Antarctica (Gallée and Schayes, 1994; Gallée et al., 2013) but have never been evaluated against *in situ* observations over the Greenlandic tundra. In this study, the MAR 3.12 version is used. With respect to version 3.11 described in detail in Kittel et al. (2021) and Amory et al. (2021), MAR v3.12 now uses the standard Polar stereographic projection EPSG 3413, corrects an important bug impacting the snow temperature at the base of the snowpack, imposes the conservation of water mass in the soil impacting notably water fluxes over the tundra and uses a continuous conversion from rainfall to snowfall from 0°C to -2°C as input of the snow model instead as a fixed one of -1°C.

As being an RCM, MAR needs to be forced with a large-scale model output such as reanalysis or ESM outputs. Large-scale conditions are prescribed every 6 hours at the MAR boundaries (temperature, specific humidity, zonal and meridional wind speeds) at each vertical level and at the surface level (pressure, sea surface temperature and sea ice concentration). A supplementary nudging is applied at the top of the atmosphere by forcing MAR with temperature and wind fields from the large-scale model in the stratosphere (Agosta et al., 2019).

3.4 MAR simulations, reanalysis and ESM outputs

For the evaluation of its wind speed outputs, the sub-region of the study area (see Fig. 2) was extracted from MAR simulations run at 15 km resolution from 2015 to 2021 at an hourly scale over the whole of Greenland. 2015 was considered as spin-up. With the aim of validating, MAR was 6 hourly forced with the ERA-5 reanalysis which is the fifth generation of global atmospheric reanalyses produced by the European Centre of Medium-Range Weather Forecasts (ECMWF) (Hersbach et al., 2020). In contrast to its predecessors ERA-40 and ERA-Interim, ERA-5 has a finer spatial resolution (31 km compared with 80 km for ERA-Interim), hourly outputs and more vertical layers (137 extending from surface to 0.01 hPa pressure level). The ERA-5 products, which are updated every three months, are currently available from 1950 to the present day. This reanalysis was chosen because, according to Delhasse et al. (2020), it is the best choice to force initial and boundary conditions of MAR. This simulation will be referred to as MAR-eval hereafter (see Table 2).

To assess future wind speed and wind power changes, five MAR simulations have been carried out at 15 km resolution over the whole of Greenland at a daily scale with five different forcing fields for 1981-2100 selected from the CMIP6. The sub-region of the study area (Fig. 2) was extracted thereafter. The ESMs used here as forcing fields are CESM2, CNRM-CM6, CNRM-ESM2, MPI-ESM1-2-HR and UKESM1-0-LL. These ESMs, already used in Hofer et al. (2020), were selected for their availability of 6-hourly outputs required to force MAR and their ability to represent the current climate over Greenland as discussed in Hofer et al. (2020). From 1981 to 2015, the ESMs were run under the Historical scenario. From 2016 to 2100, their forcing scenario is SSP5-8.5 (O'Neill et al., 2016). This scenario projects an increase in radiative forcing of 8.5 W/m^2 by 2100 and has been chosen here to enable the estimation of the extent to which the wind speed field of South Greenland could vary with the largest climate change. To serve as reference for the ESMs forced MAR simulations, a sixth simulation was produced by forcing MAR with ERA-5, this time at a daily scale, from 1981 to 2010 (present). All simulations are summarised in Table 2.

3.5 Evaluation of the MAR wind speed

In order to evaluate the performance of MAR when forced by ERA-5 to simulate wind speed above Cape Farewell, the model outputs have been compared to the wind speed observations described in Section 3.2. A methodology, described in the Supplement, was designed to choose the corresponding MAR grid pixel for each station and to check for potential outliers caused by instrumental problems that could alter the results. Statistics for annual and seasonal time series (winter and summer) were then calculated to evaluate MAR. All the results of this evaluation are listed and described in the Supplement (Section S.1). To sum up, it appears that even at 15 km of spatial resolution, MAR correlates well with the observations (R>0.70) with relatively small bias and RMSE. However, the MAR performance was locally worse over the tundra around Cape Farewell, as suggested from the statistics calculated for the stations ANG, KAT_0460 and KAT_6640 because at the resolution of 15 km, MAR is not able to resolve the fjords impacting a lot on the measured wind at these locations. A MAR simulation at higher resolution (5 km) improves a lot the comparison with these stations suggesting that the main bias here is due to the spatial resolution used in this study. Due to computing facilities, projection at resolution of 5 km was too time consuming and therefore not doable explaining why a resolution of 15km has been used here. Finally, the same statistics were computed between hourly wind gust values (3-second highest wind speed) recorded by DMI stations and regular 10m-modelled wind speed. It turns out that, although slightly underestimated, MAR could capture wind speed maxima at an hourly scale relatively well.

3.6 Methodology of analysis of wind speed anomalies and changes

3.6.1 Spatial wind speed anomalies and changes

Before assessing the two-dimensional future wind speed changes by comparing future mean wind speeds to present ones, the five ESM-forced simulations are evaluated against MAR-ERA5-ref to assess their accuracy in representing the current climate. Annual and seasonal wind speed anomalies of the ESM-forced simulations were computed by comparing them to the reference ERA5-forced simulation over the present climate. Therefore, the 1981-2010 mean wind speeds of the five ESM-forced simulations were compared to the 1981-2010 mean wind speed of MAR-ERA5-ref. The mean wind speeds were calculated at 100 m a.g.l. as it is close to hub height and to the katabatic wind speed maximum of Greenland (Heinemann, 1999). On the other hand, the future wind speed changes (annual and seasonal) were computed at 100 m a.g.l. as well by comparing the 2071-2100 mean wind speed of each ESM-forced simulation with their corresponding 1981-2010 mean wind speed. The future wind speed changes can be considered significant if their magnitude is greater than the inter-annual variability, here represented by the 1981-2010 standard deviation of annual or seasonal wind speed. As for ESM-forced wind speed anomalies over current climate, they are considered significant in regard to the 1981-2010 standard deviation of MAR-ERA5-ref. Areas of significant anomaly mean the simulation substantially overestimates (or underestimates) the wind speed compared to the reality.

3.6.2 Time series over 120 years (1981-2100)

In order to quantify the general wind speed change over South Greenland between 1981 and 2100 (annual and seasonal), spatially-averaged wind speed changes per grid cell category (ocean, tundra, ice sheet) have been calculated with the help of a linear regression. The mean wind speed of each category was calculated based on an average of all ESM-forced MAR simulations. In addition to quantifying

Time range	Forcing field	Name of simulation	Time-step
2015-2021	ERA-5	MAR-eval	hourly
1981-2010	ERA-5	MAR-ERA5-ref	daily
1981-2100	CESM2	MAR-csm	daily
1981-2100	CNRM-CM6	MAR-crmc	daily
1981-2100	CNRM-ESM2	MAR-crme	daily
1981-2100	MPI-ESM1-2-HR	MAR-mpi	daily
1981-2100	UKESM1-0-LL	MAR-uksm	daily

Table 2: List of the different MAR simulations forced with the ensemble of CMIP6 ESMs and the reanalysis ERA-5 used for the evaluation of long-term wind speed variability and validation of MAR. Note the difference in time range between MAR-eval, MAR-ERA5-ref and the other runs.

the general wind speed change over South Greenland, the change in maximum wind power that can be yielded by wind turbines was calculated thanks to the Betz equation, as described below:

$$P_{max} = (16/27) \times 0.5 \times \rho \times S \times v^3 \tag{1}$$

where P_{max} is the theoretical maximum wind power that a wind turbine can yield in W, ρ is the air density in kg/m$^{\mathbf{3}}$, S is the surface swept by the blade of the turbine in m$^{\mathbf{2}}$ and v is the wind speed in m/s. The Betz equation was applied to the daily wind speed and air density of each ESM-forced simulation between 1981 and 2100. It should be noted that S has here been fixed to 1.0, thus avoiding any effect relevant to the size of the turbine blade. Once P_{max} has been calculated for each day, the mean yearly P_{max} was calculated for each simulation for grid cell categories of tundra and ocean. The ice sheet has not been taken into account here because it is unsuitable terrain for the establishment of onshore wind turbines

4 Results

4.1 Spatial wind speed anomalies and changes

The wind speed anomalies between the five ESM-forced simulations and MAR-ERA5-ref are illustrated together with the mean anomaly in Fig. 3. The seasonal anomalies (Fig. S.1 and Fig. S.2, in Supplement) are similar to the annual anomalies with the greatest (positive) anomaly in magnitude being situated at the very southern tip of Greenland. In general, most of the study area has non-significant wind speed anomalies. Moreover, when averaged, these anomalies compensate each other so that the mean anomaly is never significant. This means that the ESM-forced simulations are reliable in representing the current wind speed field and can therefore be considered reliable to simulate the future wind speed field, taking into account the chosen SSP scenario under which they are run.

For the end of this century (2071-2100), MAR projects a significant decrease of mean annual and winter wind speed (Fig. 4.f and Fig. 6.f), especially over the tundra on the eastern side of Greenland and over Cape Farewell. Along the western coast, a wind speed decrease is more marked at the winter scale (Fig. 6.f) than at the annual scale (Fig. 4.f). On the contrary, MAR projects an increase of the summer wind speed over the ice sheet margins (Fig. 5), especially over the western side where significant positive changes are projected (Fig. 5.f). Finally, at the annual scale, a significant area of wind speed decrease is noticeable in the middle of the GrIS in Fig. 4. This area of decrease is however less clear at the seasonal scale.

4.2 Wind speed and wind power changes between 1981 and 2100

Between 1981 and 2100, the spatially-averaged yearly wind speed over the ice sheet, the tundra and the ocean is projected to decrease (Fig. 7). The wind speed over the tundra is lower than over the ice sheet because of smaller slopes and higher surface roughness which slow down the katabatic winds flowing down the ice sheet (van den Broeke et al., 1994; Ettema et al., 2010a). A general wind speed decrease, which accentuates around 2020 before stabilising around 2040, is visually noticeable on all three time series at annual and seasonal scale. This decrease is then projected to strengthen again around 2060 for winter wind speeds until 2080. For this season, the wind speed change is much stronger than in summer, especially over the tundra and the ocean (Fig. 7). The quantification of the changes calculated thanks to a linear regression is given in Table 3. Over 120 years from 1981 to 2100, the annual wind speed is suggested to decrease by ∼-0.7 m/s over the ice sheet and by ∼-0.8 m/s over the ocean and the tundra. In summer, these numbers are ∼-0.4 m/s for the ice sheet and the ocean and ∼-0.3 m/s for the tundra while in winter, the wind speed changes are ∼-0.6 m/s over the ice sheet, ∼-1.3 m/s over the ocean and ∼-0.9 m/s over the tundra. Again, these numbers highlight the stronger winter wind speed decrease over the tundra and the ocean (around three-times as much as in summer) compared to the ice sheet. The decreasing trends in wind speed can be considered significant (p-value <0.001, see Table 3).

The change in the potential maximum wind power a turbine can yield is shown in Fig. 8 for ocean and tundra based on yearly and seasonal values of maximum wind power (the ice sheet has not been considered here as it is unsuitable ground for wind farm establishment). As a reminder, the maximum wind power has been computed from daily values of wind speed and air density. The air density change is

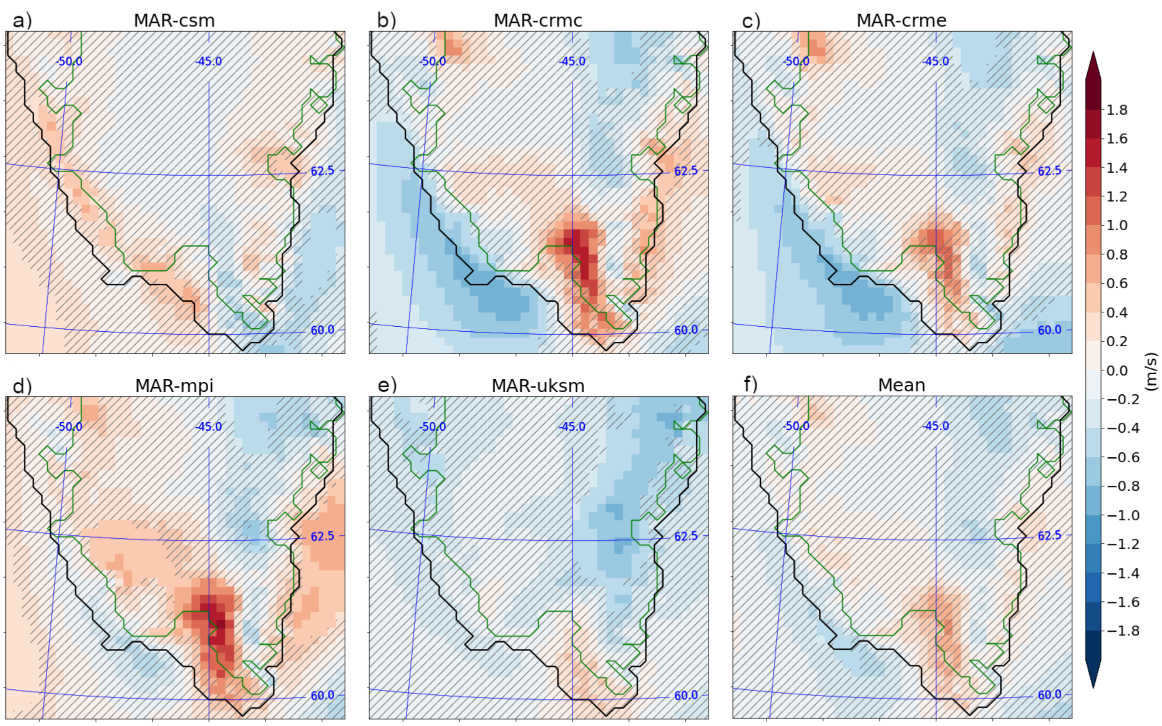

Figure 3: Wind speed anomaly between the five ESM-forced simulations and MAR-ERA5-ref from 1981-2010. The hatched area represents the regions where the anomaly is not significant in regard to the inter-annual variability of MAR-ERA5-ref. The modelled shore line (black), ice sheet contour (green) and longitudes/latitudes (blue) are represented by solid lines. The subplot f) is the mean anomaly of the five simulations

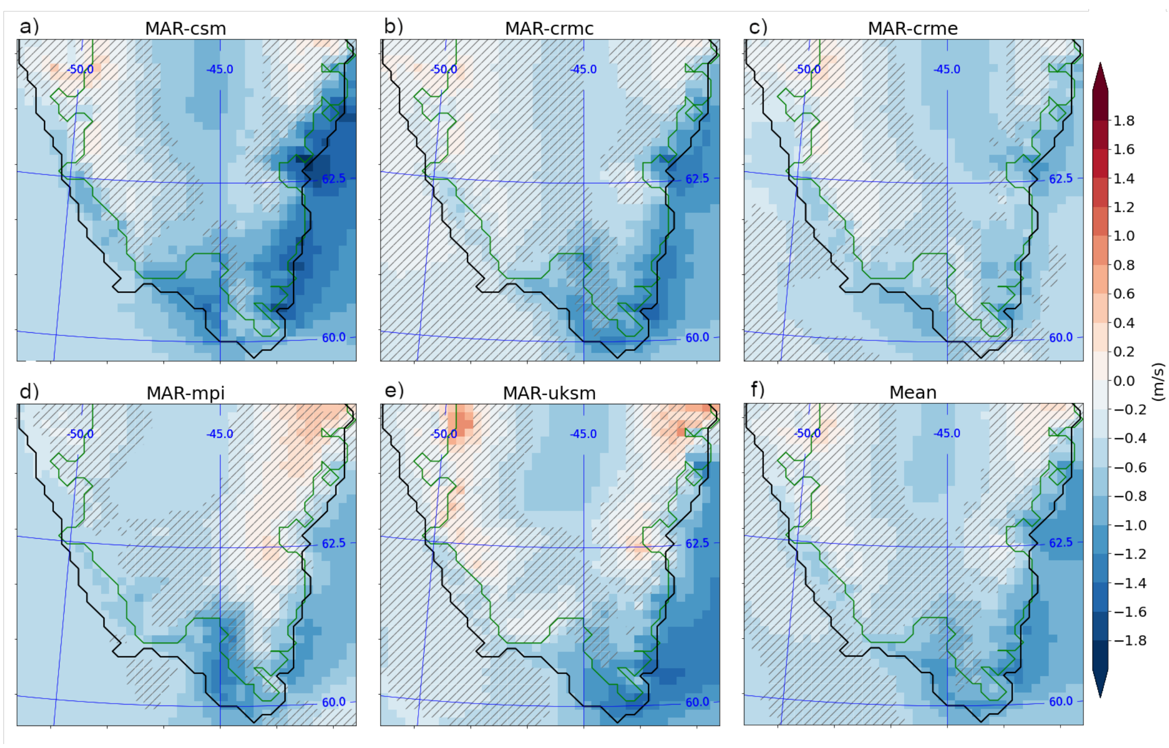

Figure 4: Projected mean yearly wind speed changes from 2071-2100 compared to 1981-2010. The hatched part represents the region where the change is insignificant with regard to the yearly present-day inter-annual variability. The modelled shore line (black), ice sheet contour (green) and longitudes/latitudes (blue) are represented by solid lines. The subplot f) is the mean anomaly of the five simulations.

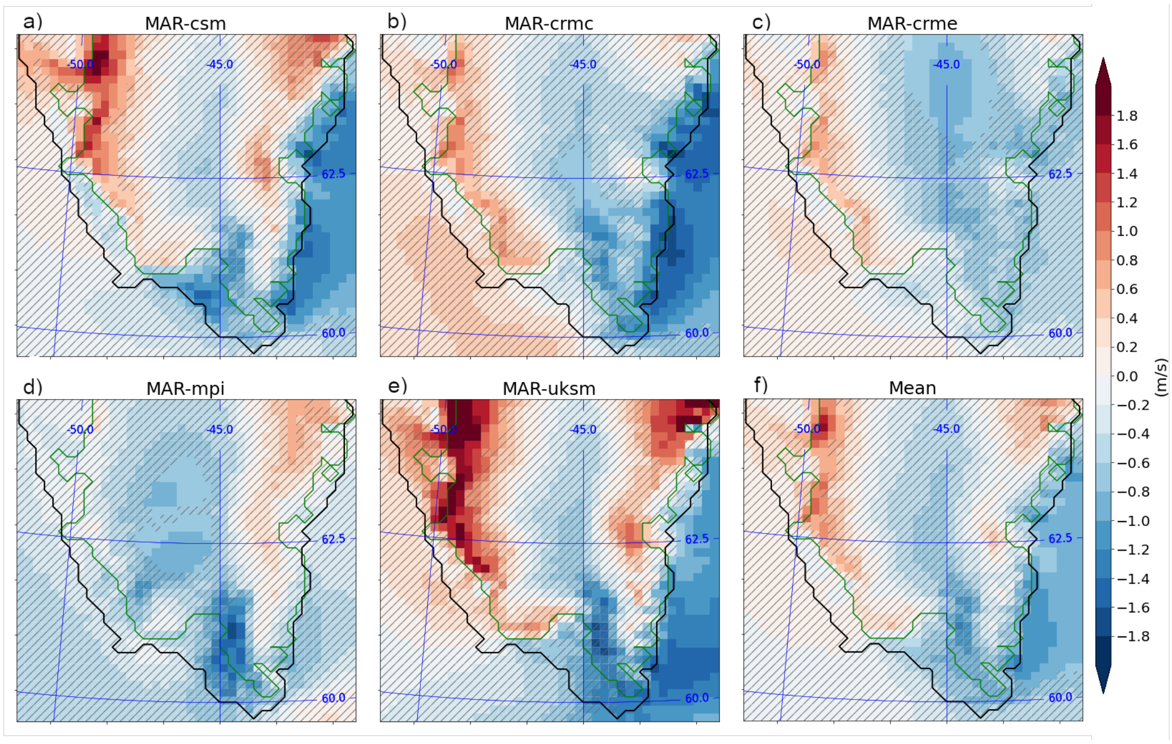

Figure 5: Projected mean summer wind speed changes (JJA) from 2071-2100 compared to 1981-2010. The hatched part represents the region where the change is insignificant with regard to the summer present-day inter-seasonal variability. The modelled shore line (black), ice sheet contour (green) and longitudes/latitudes (blue) are represented by solid lines. The subplot f) is the mean anomaly of the five simulations.

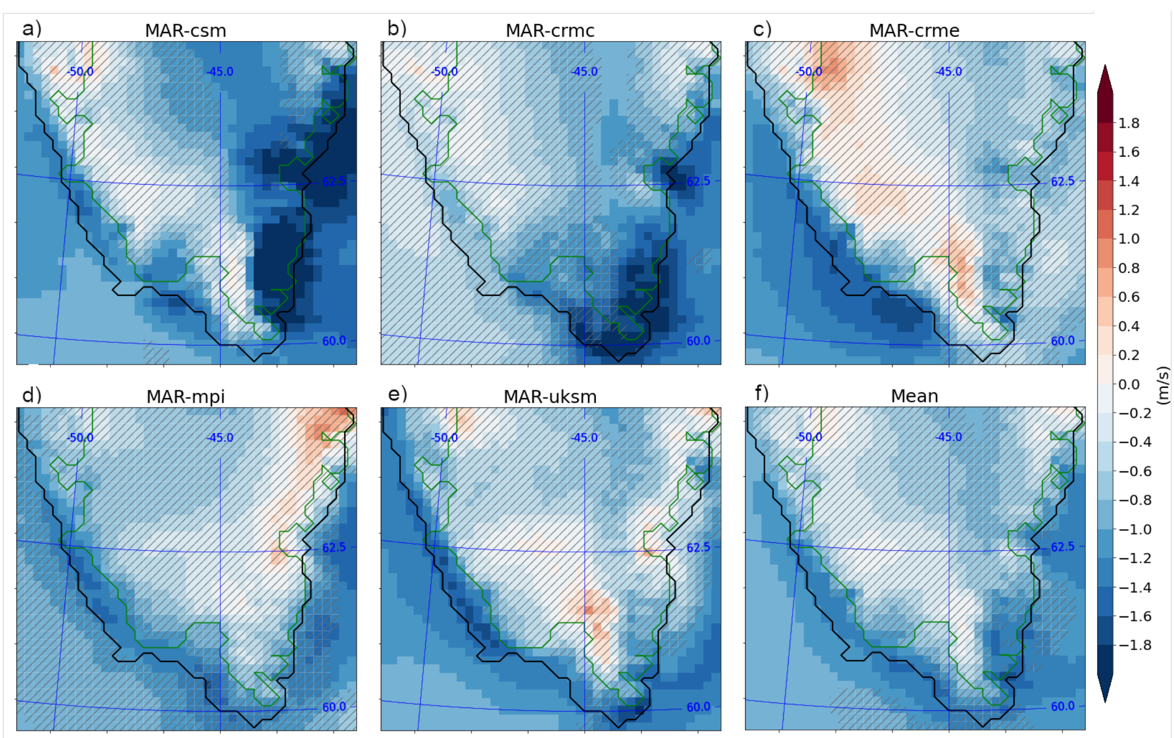

Figure 6: Projected mean winter wind speed changes (DJF) from 2071-2100 compared to 1981-2010. The hatched part represents the region where the change is insignificant with regard to the winter present-day inter-seasonal variability. The modelled shore line (black), ice sheet contour (green) and longitudes/latitudes (blue) are represented by solid lines. The subplot f) is the mean anomaly of the five simulations.

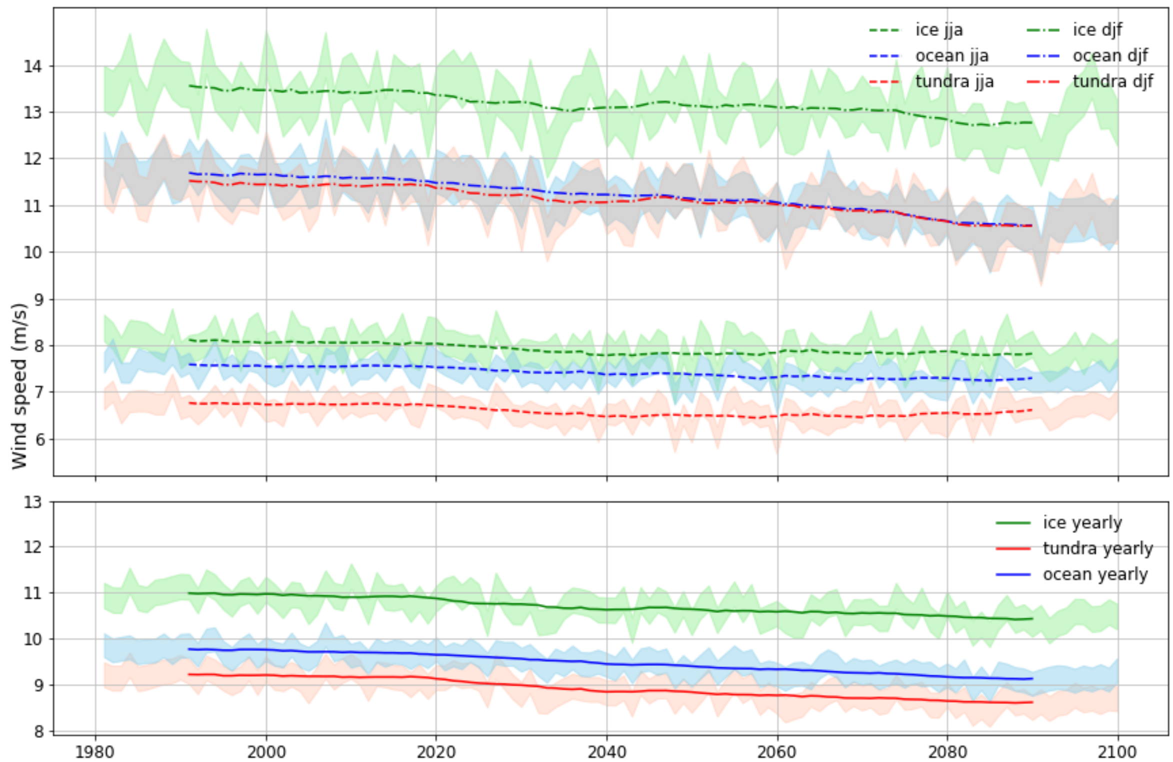

Figure 7: Wind speed time series between 1981 and 2100 averaged over the ice sheet (green), the ocean (blue) and the tundra (red). A 10-year rolling mean has been applied to the time series. Solid, dashed and dash dotted lines respectively represent the yearly, summer (JJA) and winter (DJF) wind speed. The coloured bands represent the inter-annual variability

Time period	Grid cell category	Mean wind speed of 1981-2010 (m/s)	Wind speed change (m/s)	STD (m/s)	p-value
JJA	Ice sheet	8.09	-0.38	0.28	<0.001
JJA	Ocean	7.57	-0.40	0.22	<0.001
JJA	Tundra	6.76	-0.27	0.22	<0.001
DJF	Ice sheet	13.51	-0.84	0.49	<0.001
DJF	Ocean	11.68	-1.34	0.46	<0.001
DJF	Tundra	11.48	-1.09	0.47	<0.001
Yearly	Ice sheet	10.97	-0.67	0.28	<0.001
Yearly	Ocean	9.76	-0.80	0.26	<0.001
Yearly	Tundra	9.21	-0.77	0.27	<0.001

Table 3: Projected seasonal and yearly wind speed changes between 1981 and 2100 over ice sheet, ocean and tundra, yearly STD and p-value of the change.

Time period	Grid cell category	Mean Maximum wind power of 1981-2010 (W)	Wind power change (W)	STD (W)	p-value
JJA	Ocean	381.25	-59.49	31.32	<0.001
JJA	Tundra	396.89	-63.88	42.39	<0.001
DJF	Ocean	1207.19	-273.13	106.21	<0.001
DJF	Tundra	1590.78	-268.37	168.44	<0.001
Yearly	Ocean	801.04	-155.35	51.63	<0.001
Yearly	Tundra	983.20	-178.08	73.82	<0.001

Table 4: Projected yearly and seasonal maximum collected wind power change between 1981 and 2100 over ocean and tundra, yearly STD and p-value of the change.

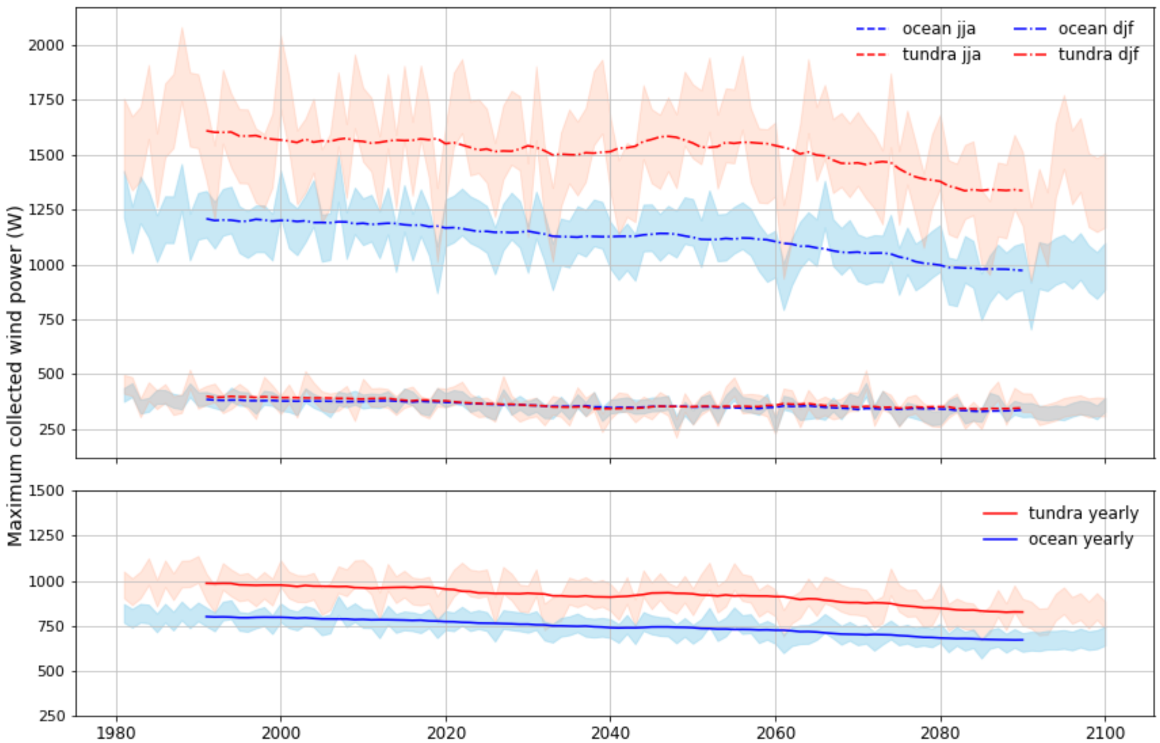

Figure 8: Maximum wind power that can be collected by a turbine between 1981 and 2100 over ocean (blue) and tundra (red), calculated with the Betz equation where the surface swept by the blade of the turbine has been set to 1.0. A 10-year rolling mean has been applied to the time series. Solid, dashed and dash dotted lines respectively represent the yearly, summer (JJA) and winter (DJF) maximum wind power. The coloured bands represent the inter-annual variability.

not shown here but it is projected to decrease due to rising temperatures over the whole study area. Combined with the decrease in wind speeds, the decrease in air density will lead to a reduction in the maximum wind power (Fig. 8). However, MAR projections surprisingly suggest a higher maximum wind power above the tundra than above the ocean despite lower wind speed and smaller density over the tundra than over the ocean. Indeed, the air density is higher over the ocean at 100 m a.g.l., because the elevation of the 100 m level above the surface is lower and the air above it contains more humidity than that above the tundra. This is likely because the Betz equation considers the cubic wind speed and was applied to daily values of wind speed and air density. Although the yearly mean wind speed is, on average, smaller for the tundra than for the ocean, the tundra experiences higher maximum daily wind speeds than the ocean (maximum daily wind speed of 32 m/s over the tundra between 1981 and 2010 versus 25 m/s for the ocean). Raised to cubic power, these events would lead to higher yearly wind power values for the tundra. The change of average yearly and seasonal wind power is listed in Table 4. The yearly change over the tundra (∼-178.1 W) is projected to be stronger than over the ocean (∼-155.4 W). This is also the case in summer (∼-63.9 W over the tundra and ∼-59.5 W over the ocean). In winter, the change is approximately four-times stronger than in summer with a decrease of ∼-268.4 W over the tundra and ∼-273.1 W over the ocean. These changes are significant with regard to their p-value. Finally, it appears from Fig. 8 that in the summer, the maximum wind power is similar over the tundra and the ocean while, on average, it becomes stronger over the tundra during winter and at the annual scale when compared with the ocean.

5 Discussion

A general wind speed decrease is projected over South Greenland by the end of the 21st century. This decrease is exacerbated in winter while in summer, areas of increased wind speed could occur along the ice sheet margins, especially on the west side. A complementary analysis of wind speed change at different vertical levels (10 m, 50 m, 500 hPa, figures in Supplement) suggests that the wind speed reduction found at 100 m a.g.l. is mainly induced by a reduction in synoptic wind speed. At 500 hPa, all simulations agree on a wind speed decrease in winter, as indicated in Fig. S.3.i where significant decrease is found. This general wind speed decrease could be explained by the Arctic Amplification. The enhanced warming in the North Pole caused by the ice albedo feedback induces an attenuation of the meridional temperature gradient between the mid-latitudes and the Poles (Jung and Schindler, 2019). However, this temperature gradient is driving the large-scale atmospheric circulation of the Northern Hemisphere so its weakening would lead to a slowing down of the synoptic dominant winds(Jung and Schindler, 2019). During winter, the large-scale temperature gradient is stronger than in summer (leading to higher wind speeds) but with the decreasing insulating sea ice cover, the ocean releases more and more heat (absorbed during sunlight days) into the cold atmosphere, enhancing the weakening of the gradient by warming the air during this season (Serreze and Francis, 2006). This would explain why the expected wind speed decrease is stronger in winter. In summer however, the simulations disagree whether the wind speed increases or decreases at 500 hPa so the evidence of synoptic wind speed decrease is less clear for this season. If there is no more sea ice cover left during summer due to global warming under scenario SSP5-8.5, the large-scale temperature gradient is no longer influenced by sea surface albedo changes during this season. The link between the projected rising air temperature and decreasing wind speeds is supported by Fig. 9 in which all simulations agree that a higher yearly temperature anomaly at 500 hPa correlates with an amplified negative yearly wind speed anomaly at 100 m a.g.l.

Furthermore, the increase in summer wind speed at the edges of the ice sheet margins by 2100 can be explained by the strengthening of the air temperature gradient between the tundra and the ice sheet. With global warming, the temperature over the tundra is projected to increase over time while the temperature of the ice sheet cannot rise above melting point. Over the ablation zone of the ice sheet, the air is cooled by the melting snow and ice. On the contrary, the heating of the air above the tundra is not limited by the presence of snow or ice during summer, reinforcing the temperature contrast between the two areas (Franco et al., 2013; Gorter et al., 2014). Fig. 10 displays the 30-year mean air temperature change simulated by MAR between 1981-2010 and 2071-2100. The rise of the temperature at 2 m a.g.l. is limited over the ice sheet margins while it reaches approximately +5°C over the tundra under emission scenario SSP5-8.5. As explained in Section 2, the temperature gradient between the ice sheet and the surrounding tundra generates a horizontal pressure gradient that drives the formation of katabatic winds. As a consequence of this gradient strengthening, the katabatic forcing above the ice sheets edges is stronger and leads to higher wind speeds in summer.

Although at 100 m a.g.l., areas of wind speed decrease in summer are not significant, at 10 m a.g.l., a marginally significant wind speed decrease is noticeable in the middle of the ice sheet (Fig. S.3.b). This might be explained by a small reduction in the katabatic forcing induced by an increase in surface roughness. With the temperature rising, the ice sheet would experience more melt and thus have more run-off water flowing over it (Fettweis et al., 2017). In the upper part of the ice sheet, mostly covered in snow where the surface roughness is less than in the ablation zone, this increased surface run-off would enhance the surface roughness as parametrized in MAR and slow down the katabatic winds by creating drainage channels (Lefebre et al., 2003; Greuell and Konzelmann, 1994).

Considering these findings, the decreasing wind speed in winter by 2100 could be beneficial for renewable electricity

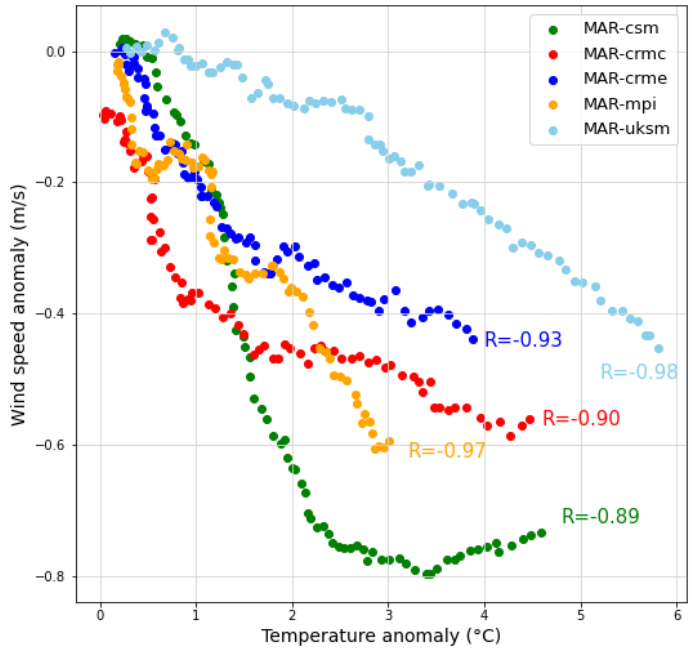

Figure 9: Projected yearly wind speed anomalies (with regard to the 1981-2010 mean wind speed) at 100 m a.g.l versus the projected yearly air temperature anomalies at 500 hPa (with regard to the 1981-2010 mean air temperature) of each ESM-forced simulation between 1981 and 2010. A 20-year rolling mean has been applied on the wind speed anomaly and temperature anomaly time series.

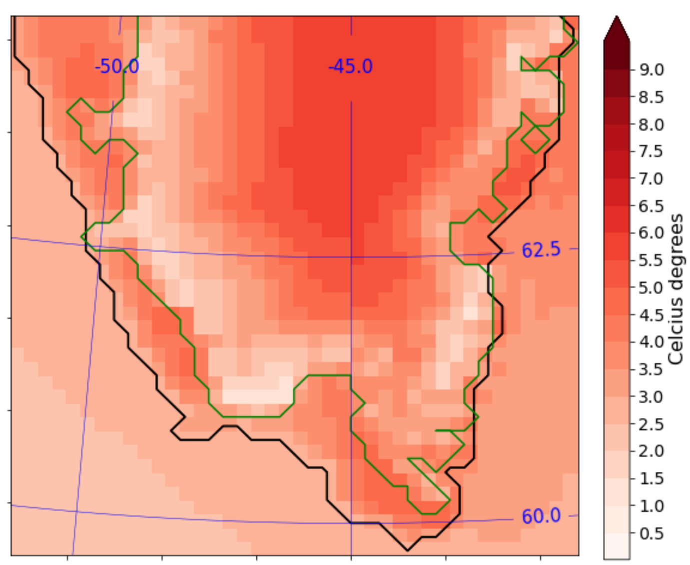

Figure 10: Projected mean air temperature change at 2 m a.g.l. Between 1981-2010 and 2071-2100, derived from an average of five ESM-forced simulations of MAR under emission scenario SSP5-8.5. The modelled shore line (black), ice sheet contour (green) and longitudes/latitudes (blue) are represented by solid lines.

production. During this season, very high wind speeds (up to 30 m/s on average) occur over the tundra in South Greenland which can exceed the cut-out speed of wind turbines (about 25 m/s but it depends on the turbine model), leading to discontinuous energy production (Radu et al., 2019). The projected winter wind speed trend suggests that the cut-out speed threshold would be less and less often surpassed (although in the future, improvements in wind turbines technology might avoid this wintertime energy-generation disruption). However, one limitation of this study is that projected wind speed trends have been investigated on seasonally and annually averaged wind speeds. To assess this hypothesis, an analysis of the occurrence of extreme wind speed events by the end of the 21st century should be conducted with regard to the cut-out speed threshold overtaking of wind turbines and is suggested as further work. Moreover, the daily wind speeds that might lead to wind turbines cut-off have not been removed from the times series used to calculate the potential maximum wind power with the Betz equation (1).

6 Conclusions

This work has aimed to answer how the wind speed over South Greenland is expected to change by 2100. Therefore, an evaluation of MAR was first performed by comparing its hourly wind speed outputs at 15 km with observations from KATABATA, DMI and PROMICE automatic weather stations in order to assess the model reliability to simulate wind speeds over the tundra in South Greenland. It turned out that MAR could accurately represent wind speed at that time and spatial resolution, although the smoothing of the topography by the model resolution used here (15 km) induced some significant local biases over the tundra.

As for the investigation of future wind speed changes, it was found that a general wind speed decrease is projected to occur by 2100 over South Greenland. This decrease might be primarily explained by a weakening of the Northern Hemisphere meridional temperature gradient that drives large-scale atmospheric circulation as a consequence of the Arctic Amplification. Nonetheless in summer, because the ice temperature cannot rise above melting point, cooling its subjacent air-layers, the katabatic forcing is likely increased at the ice sheet margins. With greater temperature contrasts between the tundra and ice sheet in summer, the pressure gradient driving katabatic wind formation is reinforced.

Despite an increase in katabatic winds in the summer, it is still projected that the wind energy that can be collected by wind turbines during this season will be less, even if not by a large amount, in 2100 than nowadays. However, it is projected that this decrease in wind energy collected will be approximately four-times stronger in the winter that in the summer. We note that this decrease in wind energy production is caused both by a decrease in wind speed and in air density.

In light of the findings from this study, further investigation should be conducted about the effects these projected changes in wind speed over the Greenlandic tundra might have on effective and efficient wind turbine functioning. Nonetheless, the projected wind speed decrease in winter might be beneficial for wind turbines as it suggests less frequent high wind speeds that might negatively affect the electricity production by cutting off the turbines. This should however be investigated deeper in detail by analysing long-term trends of high wind speeds frequency, while taking into account the continuous developments in wind turbine technology to increase their cut-out speed.

Acknowledgements

Computational resources used to perform MAR simulations have been provided by the Consortium des Équipements de Calcul Intensif (CÉCI), funded by F.R.S.-FNRS under grant 2.5020.11 and the Tier-1 supercomputer (Zenobe) of the Fédération Wallonie Bruxelles infrastructure funded by the Walloon Region under grant agreement no. 1117545. This work been supported by the European H2020 project PolarRES under grant no. 101003590.

The authors thank the University of Liège for having funded the KATABATA project, Alison Delhasse for proof reading the manuscript and giving writing advice and David Dundas for english spell and grammar revision. CL is funded by the European PolarRES project.

Data availability

The main KATABATA hourly measurement as well as the main MAR outputs are available on Zenodo (10.5281/zenodo.6055786) and the modelled data sets presented in this study are also available from the authors upon request and without conditions.

Data from the Programme for Monitoring of the Greenland Ice Sheet (PROMICE) were provided by the Geological Survey of Denmark and Greenland (GEUS) at http://www.promice.dk and were downloaded on 25/10/21 from https://promice.org/PromiceDataPortal/api/download/f24019f7-d586-4465-8181-d4965421e6eb/v3/hourly/csv.

Data from the Danish Meteorological Insitute were downloaded from https://dmiapi.govcloud.dk/ on 20/10/21.

Authors contribution

CL and XF concieved the study. CL analysed the data and led the writing of the manuscript. XF performed the MAR simulations. CL, XF and CK discussed the results. XF and DE created the KATABATA project. MF led the KATABATA expedition in Greenland to install the 3 weather stations. All co-authors revised and contributed to the editing of the manuscript.

Competing interests

The authors declare that they have no conflict of interest.

References

Agosta, C., Amory, C., Kittel, C., Orsi, A., Favier, V., Gallée, H., van den Broeke, M. R., Lenaerts, J., van Wessem, J. M., van de Berg, W. J., et al. (2019). Estimation of the Antarctic surface mass balance using the regional climate model MAR (1979–2015) and identification of dominant processes. *The Cryosphere*, 13(1):281–296.

Amory, C., Kittel, C., Le Toumelin, L., Agosta, C., Delhasse, A., Favier, V., and Fettweis, X. (2021). Performance of MAR (v3. 11) in simulating the drifting-snow climate and surface mass balance of Adelie land, East Antarctica. *Geoscientific Model Development*, 14(6):3487–3510.

Berger, M., Radu, D. C., Detienne, G., Deschuyteneer, T., Richel, A., and Ernst, D. (2021). Remote renewable hubs for carbon-neutral synthetic fuel production. *Frontiers in Energy Research*.

Bromwich, D. H., Cassano, J. J., Klein, T., Heinemann, G., Hines, K. M., Steffen, K., and Box, J. E. (2001). Mesoscale modeling of katabatic winds over Greenland with the Polar MM5. *Monthly Weather Review*, 129(9):2290–2309.

Cappelen, J., Jørgensen, B. V., Laursen, E. V., Stannius, L. S., and Thomsen, R. S. (2001). The observed climate of Greenland, 1958-99 – with climatological standards normals, 1961-90. Technical Report 00-18, Danish Meteorological Institute, Ministery of Transport, Copenhagen,Danemark.

Chatzivasileiadis, S., Ernst, D., and Andersson, G. (2013). The global grid. *Renewable Energy*, 57:372–383.

da Silva Soares, J. P. (2016). Wind energy utilization in Arctic climate - RACMO 2.3 Greenland Climate Runs Project. Master's thesis, Uppsala University, Sweden.

De Ridder, K. and Gallée, H. (1998). Land surface–induced regional climate change in southern Israel. *Journal of applied meteorology*, 37(11):1470–1485.

Delhasse, A., Kittel, C., Amory, C., Hofer, S., van As, D., Fausto, R. S., and Fettweis, X. (2020). Brief communication: Evaluation of the near-surface climate in ERA5 over the Greenland Ice Sheet. *The Cryosphere*, 14(3):957–965.

Ettema, J., van den Broeke, M. R., van Meijgaard, E., and Van de Berg, W. J. (2010a). Climate of the Greenland ice sheet using a high-resolution climate model–Part 2: Near-surface climate and energy balance. *The Cryosphere*, 4(4):529–544.

Ettema, J., van den Broeke, M. R., van Meijgaard, E., Van de Berg, W. J., Box, J. E., and Steffen, K. (2010b). Climate of the Greenland ice sheet using a high-resolution climate model–Part 1: Evaluation. *The Cryosphere*, 4(4):511–527.

Fausto, R. S., van As, D., Mankoff, K. D., Vandecrux, B., Citterio, M., Ahlstrøm, A. P., Andersen, S. B., Colgan, W., Karlsson, N. B., Kjeldsen, K. K., et al. (2021). Programme for Monitoring of the Greenland Ice Sheet (PROMICE) automatic weather station data. *Earth System Science Data*, 13(8):3819–3845.

Fettweis, X., Box, J. E., Agosta, C., Amory, C., Kittel, C., Lang, C., van As, D., Machguth, H., and Gallée, H. (2017). Reconstructions of the 1900–2015 greenland ice sheet surface mass balance using the regional climate mar model. *The Cryosphere*, 11(2):1015–1033.

Fettweis, X., Franco, B., Tedesco, M., Van Angelen, J. H., Lenaerts, J. T. M., van den Broeke, M. R., and Gallée, H. (2013). Estimating the Greenland ice sheet surface mass balance contribution to future sea level rise using the regional atmospheric climate model MAR. *The Cryosphere*, 7(2):469–489.

Fettweis, X., Hofer, S., Krebs-Kanzow, U., Amory, C., Aoki, T., Berends, C. J., Born, A., Box, J. E., Delhasse, A., Fujita, K., et al. (2020). GrSMBMIP: intercomparison of the modelled 1980–2012 surface mass balance over the Greenland Ice Sheet. *The Cryosphere*, 14(11):3935–3958.

Franco, B., Fettweis, X., and Erpicum, M. (2013). Future projections of the Greenland ice sheet energy balance driving the surface melt. *The Cryosphere*, 7(1):1–18.

Franco, B., Fettweis, X., Lang, C., and Erpicum, M. (2012). Impact of spatial resolution on the modelling of the Greenland ice sheet surface mass balance between 1990–2010, using the regional climate model MAR. *The Cryosphere*, 6(3):695–711.

Gallée, H. and Schayes, G. (1994). Development of a three-dimensional meso-γ primitive equation model: katabatic winds simulation in the area of Terra Nova Bay, Antarctica. *Monthly Weather Review*, 122(4):671–685.

Gallée, H., Trouvilliez, A., Agosta, C., Genthon, C., Favier, V., and Naaim-Bouvet, F. (2013). Transport of snow by the wind: A comparison between observations in Adélie Land, Antarctica, and simulations made with the regional climate model MAR. *Boundary-layer meteorology*, 146(1):133–147.

Gorter, W., Van Angelen, J. H., Lenaerts, J. T. M., and van den Broeke, M. R. (2014). Present and future near-surface wind climate of Greenland from high resolution regional climate modelling. *Climate dynamics*, 42(5-6):1595–1611.

Greuell, W. and Konzelmann, T. (1994). Numerical modelling of the energy balance and the englacial temperature of the Greenland Ice Sheet. Calculations for the ETH-Camp location (West Greenland, 1155 m asl). *Global and Planetary change*, 9(1-2):91–114.

Hanna, E., Cappelen, J., Fettweis, X., Mernild, S. H., Mote, T. L., Mottram, R., Steffen, K., Ballinger, T. J., and Hall, R. J. (2021). Greenland surface air temperature changes from 1981 to 2019 and implications for ice-sheet melt and mass-balance change. *International Journal of Climatology*, 41:E1336–E1352.

Heinemann, G. (1999). The KABEG'97 field experiment: An aircraft-based study of katabatic wind dynamics over the Greenland ice sheet. *Boundary-Layer Meteorology*, 93(1):75–116.

Hersbach, H., Bell, B., Berrisford, P., Hirahara, S., Horányi, A., Muñoz-Sabater, J., Nicolas, J., Peubey, C., Radu, R., Schepers, D., et al. (2020). The ERA5 global reanalysis. *Quarterly Journal of the Royal Meteorological Society*, 146(730):1999–2049.

Hofer, S., Lang, C., Amory, C., Kittel, C., Delhasse, A., Tedstone, A., and Fettweis, X. (2020). Greater Greenland Ice Sheet contribution to global sea level rise in CMIP6. *Nature communications*, 11(1):1–11.

Jakobsen, K. R. (2016). *Renewable energy potential of Greenland with emphasis on wind resource assessment*. PhD thesis, Technical University of Danemark, Danemark.

Jung, C. and Schindler, D. (2019). Changing wind speed distributions under future global climate. *Energy Conversion and Management*, 198:111841.

Kittel, C., Amory, C., Agosta, C., Jourdain, N. C., Hofer, S., Delhasse, A., Doutreloup, S., Huot, P.-V., Lang, C., Fichefet, T., et al. (2021). Diverging future surface mass balance between the Antarctic ice shelves and grounded ice sheet. *The Cryosphere*, 15(3):1215–1236.

Klein, T. and Heinemann, G. (2002). Interaction of katabatic winds and mesocyclones near the eastern coast of Greenland. *Meteorological Applications*, 9(4):407–422.

Klein, T., Heinemann, G., Bromwich, D. H., Cassano, J. J., and Hines, K. M. (2001). Mesoscale modeling of katabatic winds over Greenland and comparisons with aws and aircraft data. *Meteorology and Atmospheric Physics*, 78(1):115–132.

Lefebre, F., Gallée, H., van Ypersele, J.-P., and Greuell, W. (2003). Modeling of snow and ice melt at ETH Camp (West Greenland): A study of surface albedo. *Journal of Geophysical Research: Atmospheres*, 108(D8).

Moore, G. W. K. and Renfrew, I. A. (2005). Tip jets and barrier winds: A QuikSCAT climatology of high wind speed events around Greenland. *Journal of Climate*, 18(18):3713–3725.

Moore, G. W. K., Renfrew, I. A., Harden, B. E., and Mernild, S. H. (2015). The impact of resolution on the representation of southeast Greenland barrier winds and katabatic flows. *Geophysical Research Letters*, 42(8):3011–3018.

O'Neill, B. C., Tebaldi, C., van Vuuren, D. P., Eyring, V., Friedlingstein, P., Hurtt, G., Knutti, R., Kriegler, E., Lamarque, J.-F., Lowe, J., et al. (2016). The scenario model intercomparison project (ScenarioMIP) for CMIP6. *Geoscientific Model Development*, 9(9):3461–3482.

Payne, A. J., Nowicki, S., Abe-Ouchi, A., Agosta, C., Alexander, P., Albrecht, T., Asay-Davis, X., Aschwanden, A., Barthel, A., Bracegirdle, T. J., et al. (2021). Future sea level change under CMIP5 and CMIP6 scenarios from the Greenland and Antarctic ice sheets. *Geophysical Research Letters*, page e2020GL091741.

Radu, D., Berger, M., Fonteneau, R., Hardy, S., Fettweis, X., Le Du, M., Panciatici, P., Balea, L., and Ernst, D. (2019). Complementarity assessment of South Greenland katabatic flows and West Europe wind regimes. *Energy*, 175:393–401.

Serreze, M. C. and Francis, J. A. (2006). The Arctic on the fast track of change. *Weather*, 61(3):65–69.

van As, D., Fausto, R. S., Steffen, K., Ahlstrøm, A. P., Andersen, S. B., Andersen, M. L., Box, J. E., Charalampidis, C., Citterio, M., Colgan, W. T., Edelvang, K., Larsen, S. H., Nielsen, S., Veicherts, M., and Weidick, A. (2014). Katabatic winds and piteraq storms: Observations from the greenland ice sheet. *Geologic survey of Danemark and Greenland Bulletin*, 31:83–86.

van den Broeke, M. R., Duynkerke, P. G., and Oerlemans, J. (1994). The observed katabatic flow at the edge of the Greenland ice sheet during GIMEX-91. *Global and Planetary Change*, 9(1-2):3–15.

Supplementary work

S.1 Evaluation of MAR wind speed outputs

The first step of the evaluation of MAR wind speed outputs was, for each station, to find the corresponding cell of the MAR grid in MAR-eval. Therefore, for each station, all the land (i.e., surface elevation greater than 0) grid cells for which the distance between their centre and the station was equal or inferior to the spatial resolution were inspected and the grid cell with the closest altitude to that of the station was kept. Wind speed, temperature and surface pressure were then extracted from MAR-eval, from 2016 to 2018 for pixels corresponding to DMI and PROMICE stations and from September 2020 to the end of August 2021 for grid cells corresponding to KATABATA stations.

Subsequently, observed hourly temperature at 2 m and hourly surface pressure (except for KATABATA stations for which it was not available) were compared with the MAR-eval temperature at 2 m and surface pressure to check for potential outliers. Therefore, KATABATA time series, which have a time-step of 20 minutes, were resampled in hourly time series by applying an hourly average. The PROMICE and DMI data were directly downloaded as hourly time series. Moreover, time-steps with erroneous data in the observed temperature and surface pressure time series were removed from the corresponding observed wind speed time series. This was carried out to account for potential instrumentation problems a station might encounter in the extreme Greenlandic climatic conditions such as sensor icing or toppling over under high-speed wind gusts (Cappelen et al., 2001). During this data inspection, it appeared that only a few time-steps had visually obvious erroneous temperature observations for IKM in 2016 and NUN in 2017. All DMI and PROMICE stations have a correlation of R>0.98 (not shown) between their measured surface pressure and the surface pressure of MAR-eval, suggesting that the stations were functioning correctly at the time. This was confirmed with the temperature correlation for which R in each case was greater than 0.88 (not shown), once the erroneous observations had been removed from the above-cited time series, namely IKS in 2016 and NUN in 2017. It should be noted that to calculate the surface pressure and temperature correlations, the MAR-eval time steps for which the corresponding observation data was missing were removed from the time series. For the KATABATA stations, because the surface pressure data was not available, only the temperature was inspected to check for potential instrumentation problems. No obvious erroneous data was visuallly found in the time series.

After time-steps with outliers and missing data were removed from both observation and MAR-eval wind speed time series, their correlation, bias, RMSE and centred RMSE (RMSEC) were calculated on the whole 3-year time series for DMI and PROMICE stations and on the available time period of the KATABATA stations. For DMI and PROMICE stations, the statistics were also calculated for summer and winter time series. Summer time series consist of the succession of the three summers (June-July-August (JJA)) of 2016, 2017 and 2018. The same goes for winters (January-February-March (JFM)). For KATABATA and DMI stations, the data was compared with simulated wind speed at 10 m a.g.l., as it is the height at which observed wind speed is measured by these stations. However, data from the PROMICE stations was compared with simulated wind speed at 2 m a.g.l.. As explained in Section 3.2, the PROMICE sensors do not measure wind speed at 10 m but rather between 0 and 3.1 m a.g.l.. Indeed, because the stations are located in an area with high snowfall accumulation, the height at which PROMICE stations record wind speed varies through the year. The yearly average height at which PROMICE stations record wind speed, derived from measured heights a.g.l., is close to 2 m and this is why this level has been chosen in MAR-eval for comparison with the PROMICE data. The results of this evaluation are listed in Table S.1 for the KATABATA stations and in Table S.2 for the DMI and PROMICE stations. It is important to keep in mind that the NAR time series only covers 2018, and the same goes for IKS which only covers 2016-2017. For DMI stations, the hourly wind gusts data were compared with MAR-eval regular 10 m hourly averaged wind speed to evaluate the capacity of MAR to simulate wind speed maxima. The regular 10 m MAR-eval hourly averaged wind speed was chosen because MAR does not simulate wind gusts. The results are listed in Table S.3.

Table S. 1: Correlation (R), bias, root mean square error (RMSE) and centered RMSE (RMSEC) between wind speed observation data from the KATABATA stations and MAR wind speed values. Note the different time ranges between stations

Station	**Statistic**	**Value**	**Time range (dd/mm/yy)**
KAT 6640	**R**	**0.59**	06/09/20 - 31/01/21
	Bias	0.88	
	RMSE	5.37	
	RMSEC	5.30	
KAT 0460	**R**	**0.56**	08/09/20 - 31/08/21
	Bias	2.43	
	RMSE	6.14	
	RMSEC	5.64	
KAT 0680	**R**	**0.83**	11/09/20 - 28/02/21
	Bias	3.84	
	RMSE	5.46	
	RMSEC	3.89	

It appears from Table S.1 that the correlation between the wind speed measured by KATABATA stations and wind speed extracted from their corresponding MAR-eval grid cells varies quite considerably between the three stations. Only KAT 0680 shows good correlation with MAR-eval (R>0.70). A 3-days running correlation was applied on the KATABATA time series to check for potential time shifts in the data. Although an offset of +2h in regard to UTC time (which is the model time) is suspected for stations KAT 0460 and KAT 0680, the correction of this offset barely improves the correlation with MAR-eval. Scatter plots of wind speed difference between a station and its MAR-eval grid cell versus temperature (observed and modelled) enable one to check for wind sensor icing that would slow down the rotation of the instrument. No evidence of such icing that could explain the poor correlations between KAT 0460 and KAT 6640 with MAR-eval could be found. As for the RMSE and centred RMSE, these were superior to one STD for KAT 0460. This means that at the location where the observations were recorded, MAR does not represent the wind speed variations well, probably because the environment in which the station is located is inadequately resolved by MAR. The bias of MAR-eval is positive for all KATABATA stations and is the strongest for KAT 0680, representing 65% of the mean observed wind speed. Again, that could be explained by the fact that KAT 0680 is located in a narrow fjord that could act as a protection/shelter from wind, that is not resolved by the model resolution. The RMSE and centred RMSE are relatively high with regard to the STD (not shown). The centred RMSE represents 116% of KAT 0460 STD, 95% for KAT 6640 and 70% for KAT 0680.

As for DMI and PROMICE stations, it appears from Table S.2 that for most stations, the yearly correlation between the observed and the modelled wind speed is good ($R>0.70$). Stations IKM and UKI have an $R=0.69$ so their yearly correlation can be considered good as well. Only station ANG shows poor yearly correlation ($R=0.55$). It should be noted that station ANG is located not very far from stations KAT 6640 and KAT 0460. This supports the fact that the poor correlation with MAR-eval for these stations is more likely linked to their location rather than to instrumentation problems. Moreover, ANG has the same MAR-eval grid cell as KAT 6640 and is only one grid cell away from KAT 0460. Such as for the latter station, ANG has a centred RMSE greater than one STD (approximately 104% of it, not shown). The poor correlations of stations ANG and KAT 6640 are likely to be due to a lack of topography resolving by the model, as was suggested by previous simulations of MAR at 5 km of spatial resolution, for which correlation with observation data were much better. As an example, the correlation between MAR and observations at 5 km is 0.81 for KAT 6640, 0.80 for KAT 0460 and 0.70 for KAT 0680 for September-December 2020, while it is 0.68 for KAT 6640, 0.71 for KAT 0460 and 0.74 for KAT 0680 at 15 km for the same period. On a seasonal basis, the correlation between the observed and the modelled wind speed is markedly improved in summer compared to winter (delta $R \geq 0.05$) for IKS, QAS_L and QAS_M.

Finally, Table S.3 lists the correlation, bias, RMSE and RMSEC between DMI measured wind gusts and MAR-eval 10 m mean wind speed at an hourly scale. Except for ANG, the correlation with MAR is greater than 0.70 for all stations, suggesting that MAR performs well in capturing wind speed maxima. The correlation for wind gusts with MAR is even slightly better than the observed 10 m mean wind speed. The bias of the model is of course negative considering that we take the modelled regular 10 m mean wind speed, as the model does not simulate wind gusts in a separate variable. The bias can represent up to 35% of the observed STD, as is the case for NUN (not shown). RMSE and centred RMSE are never greater than one STD, which means that MAR shows good performance for representing wind speed maxima.

Table S. 2: Correlation (R), bias, RMSE and centered RMSE (RMSEC) between wind speed observation data from DMI and PROMICE stations and MAR-eval wind speeds for 2016-2018. Note that these statistics have only been computed from 2016 to 2017 for IKS and only for 2018 for NAR and QAS_M.

Station	Statistic	Winter	Summer	Yearly
ANG	**R**	**0.49**	**0.46**	**0.55**
	Bias	1.90	0.35	1.01
	RMSE	6.82	4.61	5.71
	RMSEC	6.55	4.59	5.62
IKM	**R**	**0.66**	**0.70**	**0.69**
	Bias	1.09	0.14	0.88
	RMSE	4.84	2.81	4.05
	RMSEC	4.72	2.80	3.95
IKS	**R**	**0.75**	**0.81**	**0.79**
	Bias	2.47	2.05	2.52
	RMSE	5.14	3.38	4.41
	RMSEC	4.51	2.70	3.62
NAR	**R**	**0.79**	**0.82**	**0.81**
	Bias	1.45	-0.21	0.83
	RMSE	3.57	2.09	3.01
	RMSEC	3.26	2.08	2.90
NUN	**R**	**0.79**	**0.81**	**0.83**
	Bias	-2.11	-0.98	-1.57
	RMSE	4.44	2.80	3.65
	RMSEC	3.91	2.62	3.29
UKI	**R**	**0.69**	**0.71**	**0.69**
	Bias	-0.59	0.20	-0.18
	RMSE	3.59	2.48	3.28
	RMSEC	3.54	2.47	3.28
QAS_L	**R**	**0.67**	**0.59**	**0.72**
	Bias	-0.05	-0.59	-0.33
	RMSE	3.23	2.02	2.65
	RMSEC	3.23	1.93	2.63
QAS_M	**R**	**0.65**	**0.46**	**0.73**
	Bias	1.08	-0.28	0.82
	RMSE	3.37	1.76	2.81
	RMSEC	3.19	1.74	2.69
QAS_U	**R**	**0.72**	**0.74**	**0.77**
	Bias	0.65	-0.21	0.10
	RMSE	3.07	1.59	2.49
	RMSEC	3.00	1.58	2.49

Table S. 3: Correlation (R), bias, RMSE and centered RMSE (RMSEC) between wind gust observation data from DMI stations and MAR wind speed values for 2016-2018. Note that these statistics have only been computed from 2016 to 2017 for IKS and only for 2018 for NAR.

Station	Statistic	Winter	Summer	Yearly
ANG	**R**	**0.50**	**0.48**	**0.57**
	Bias	-0.58	-1.06	-1.19
	RMSE	7.39	5.12	6.23
	RMSEC	7.37	5.01	6.12
IKM	**R**	**0.69**	**0.74**	**0.72**
	Bias	-1.72	-1.47	-1.27
	RMSE	6.19	3.79	5.01
	RMSEC	5.95	3.49	4.84
IKS	**R**	**0.77**	**0.83**	**0.81**
	Bias	-3.31	-1.70	-2.20
	RMSE	7.30	4.29	5.67
	RMSEC	6.51	3.94	5.22
NAR	**R**	**0.81**	**0.86**	**0.84**
	Bias	-1.65	-2.52	-1.86
	RMSE	4.25	3.67	3.84
	RMSEC	3.91	2.67	3.36
NUN	**R**	**0.79**	**0.81**	**0.84**
	Bias	-5.55	-3.52	-4.76
	RMSE	7.55	4.98	6.50
	RMSEC	5.12	3.52	4.43
UKI	**R**	**0.69**	**0.74**	**0.72**
	Bias	-2.68	-1.29	-2.08
	RMSE	4.92	3.03	4.22
	RMSEC	4.13	2.74	3.67

S.2 Summer and Winter wind speed anomalies

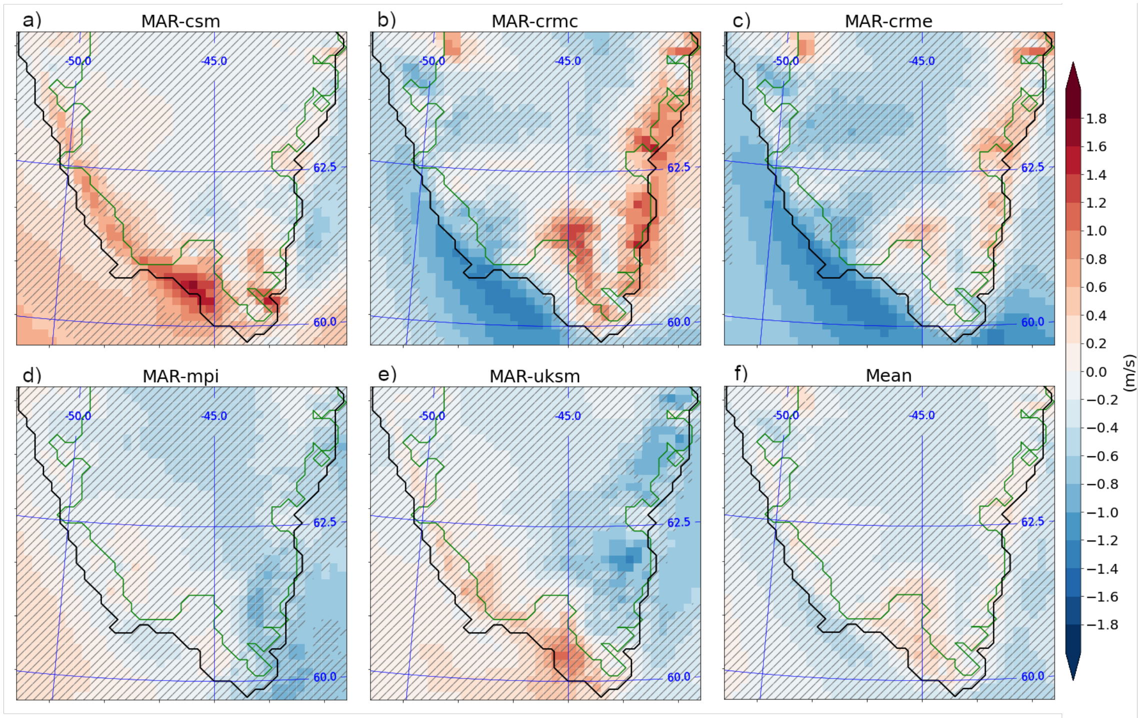

Figure S. 1: Summer wind speed anomaly (JJA) between the five ESM-forced simulations and MAR-ERA5-ref from 1981-2010. The hatched area represents the regions where the anomaly is not significant with regard to the summer inter-seasonal variability of MAR-ERA5-ref. The modelled shore line (black), ice sheet contour (green) and longitudes/latitudes (blue) are represented by solid lines. The subplot f) is the mean anomaly of the five simulations.

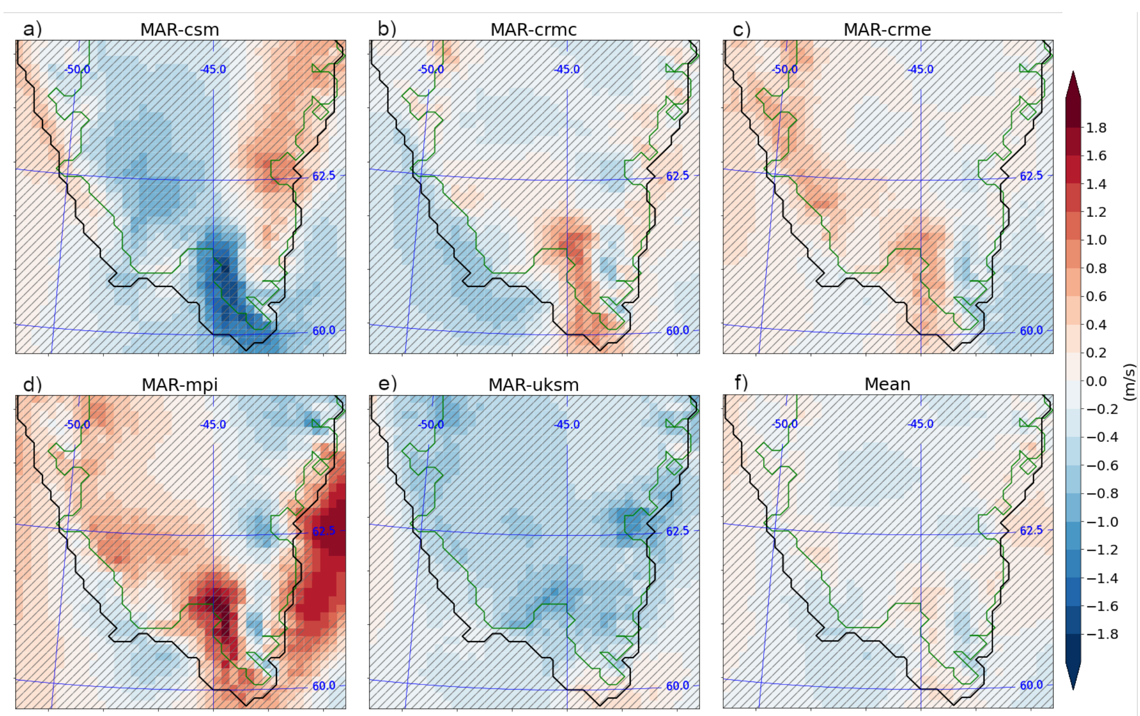

Figure S. 2: Winter wind speed anomaly (DJF) between the five ESM-forced simulations and MAR-ERA5-ref from 1981-2010. The hatched area represents the regions where the anomaly is not significant with regard to the summer inter-seasonal variability of MAR-ERA5-ref. The modelled shore line (black), ice sheet contour (green) and longitudes/latitudes (blue) are represented by solid lines. The subplot f) is the mean anomaly of the five simulations.

S.3 Multi-level mean wind speed change

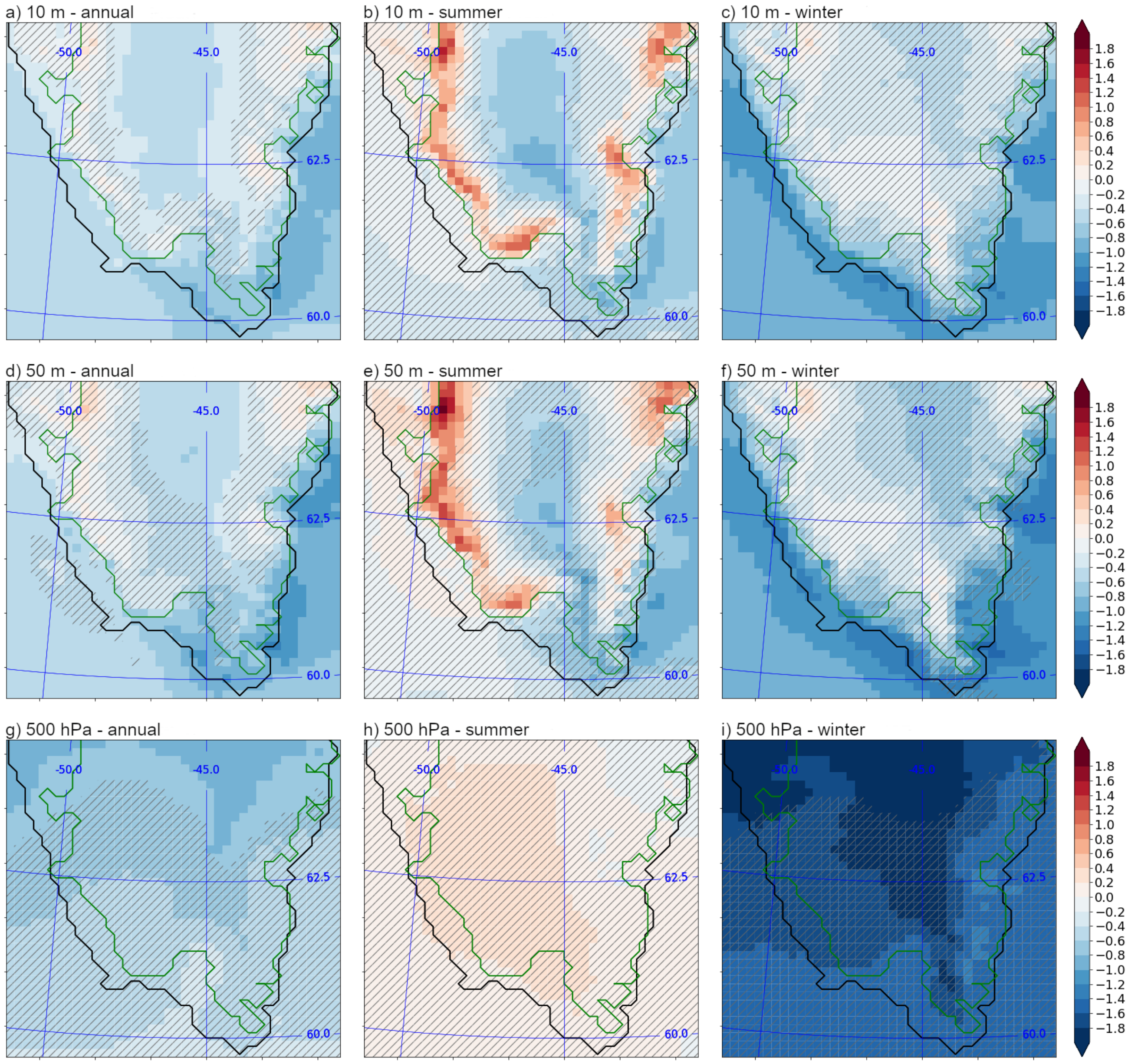

Figure S. 3: Mean projected wind speed change between 1981-2010 and 2071-2100 at 10 and 50 m a.g.l. and 500 hPa at annual and seasonal scale (JJA and DJF). Mean of all five ESM-forced MAR simulations. The modelled shore line (black), ice sheet contour (green) and longitudes/latitudes (blue) are represented by solid lines.